Tribology International 49 (2012) 17–29

Contents lists available at SciVerse ScienceDirect

Tribology International

journal homepage: www.elsevier.com/locate/triboint

Transient mixed thermo-elastohydrodynamic lubrication in multi-speed transmissions

M. De la Cruz [a], W.W.F. Chong [b], M. Teodorescu [b,c], S. Theodossiades [a,*], H. Rahnejat [a]

[a] Wolfson School of Mechanical and Manufacturing Engineering, Loughborough University, Loughborough, UK
[b] School of Engineering, Cranfield University, Cranfield, UK
[c] Baskin School of Engineering, University of California, Santa Cruz, CA USA

ARTICLE INFO

Article history:
Received 1 July 2011
Received in revised form
5 December 2011
Accepted 8 December 2011
Available online 16 December 2011

Keywords:
Multi-speed transmissions
Mixed thermo-elastohydrodynamics
Loose gear rattle

ABSTRACT

Noise, vibration and harshness (NVH) refinement as well as thermo-mechanical efficiency are the key design attributes of modern compact multi-speed transmissions. Therefore, unlike simple gear pair models, a full transmission model is required for a simultaneous study. The prominent NVH concern is transmission rattle, dominated by the intermittent unintended meshing of several lightly loaded unselected loose gear pairs arising from the system compactness. These gear pairs are subjected to hydrodynamic impacts. The thermo-mechanical efficiency is dominated by the engaged gears, with simultaneous meshing of teeth pairs subject to thermo-elastohydrodynamic regime of lubrication, with often quite thin films, promoting asperity interactions. Therefore, a full transmission model is presented, comprising system dynamics, lubricated contacts, asperity interactions and thermal balance. Generic multi-physics models of this type are a prerequisite for in-depth analysis of transmission efficiency and operational refinement. Hitherto, such an approach has not been reported in literature.

1. Introduction

Gears have played a significant role in industrial progress almost from the outset, with the recorded history bearing witness to their use as far back as 3129 BC in a potter's wheel discovered in Ur, Mesopotamia. From the very early days, friction, wear and lubrication of contacting surfaces have been the main concerns in design and use of gears. Another problem has been gear vibration, most pertinently in recent years when it has become a quality issue. This is a major preoccupation for transmission engineers, who search for palliation for a plethora of onomatopoeically named noise phenomena such as gear rattle, whine and grunt. Therefore, accurate methods of prediction for both tribological and dynamic conditions have always been sought. Of course dynamics and tribology of gears are closely intertwined.

The use of low shear strength media to reduce friction of contacting surfaces was clearly intuitive right from the dawn of transportation, such as the application of animal or vegetable fats in the rudimentary chariot wheels. However, a fundamental understanding of the underlying mechanism of elastohydrodynamic lubrication (EHL) only emerged 70 years ago with the postulate of Ertel and Grubin [1].

Prediction of conditions in tribology of gears has evolved with the improving understanding of fundamentals of elastohydrodynamic contacts, with numerical solutions for line contact configuration first obtained by Dowson and Higginson [2] and for point contacts by Cameron and Gohar [3] under assumed steady state conditions. These formed the basis for gear tribology among other concentrated counterforming contacts.

Thin elastohydrodynamic films predicted for gear meshing teeth are usually insufficient to guard against the interaction of asperities on contiguous surfaces. Therefore, a mixed regime of lubrication is often prevalent [4]. Under these circumstances both shear of the lubricant film and boundary interactions contribute to generated friction [5]. Additionally, for such thin films viscous shear often exceeds the limiting Eyring shear stress of the lubricant and non-Newtonian behaviour ensues. To take these into account a number of methods have been devised, either to determine an effective coefficient of friction according to the prevailing regime of traction [6,7] or combined mixed regime of lubrication [8,5]. The generated friction causes shear thinning of the lubricant, with the effective viscosity obtained because of a corresponding rise in the contact temperature. In turn, the reduced effective viscosity of the lubricant further decreases the film thickness.

Under isothermal conditions, often assumed to somewhat reduce the complexity of numerical solutions, a combined solution of Reynolds and elasticity potential equation is sought. The solutions proposed, for example, by Li and Kahraman [9] and

* Corresponding author.
E-mail address: S.Theodossiades@lboro.ac.uk (S. Theodossiades).

0301-679X
doi:10.1016/j.triboint.2011.12.006

Nomenclature

b	Hertzian contact half width [m]
C	gear teeth and retaining bearings' clearance [m]
C_p	specific heat capacity of lubricant [$J kg^{-1} K^{-1}$]
E	Young's modulus of elasticity [Pa]
E^*	reduced modulus of elasticity [Pa]
F	friction [N]
h	lubricant film thickness [m]
h_o	undeformed rigid gap [m]
I	mass moment of Inertia [kg m^2]
k	thermal conductivity of lubricant [W K^{-1} m^{-1}]
ℓ	contact length [m]
p	pressure [Pa]
p_c	cavitation pressure [Pa]
p_H	Hertzian pressure [Pa]
p_m	mean Hertzian pressure [Pa]
Q_s^*	non-dimensional side leakage flow [dimensionless]
r,R	radius [m]
r_x	equivalent contact radius in the zx plane [m]
t	time [s]
T_D	resistive torque [N m]
$u_{av}=u$	speed of entraining motion [m s^{-1}]
v_{ppitch}	pinions' pitch velocity [m s^{-1}]
v_{wpitch}	wheels' pitch velocity [m s^{-1}]
W	contact load [N]

Greek characters

α_o	pressure–viscosity coefficient at ambient pressure and temperature [Pa^{-1}]
α_n	normal pressure angle [rad]
α_t	transverse pressure angle [rad]
β	bulk modulus of the lubricant [Pa]
β'	viscosity–temperature coefficient [°C^{-1}]
β_b	helix angle [rad]
γ	slope of the oil film limiting shear stress–pressure relationship [dimensionless]
δ	localised deflection [m]
Δu	sliding speed [m s^{-1}]
η	effective viscosity [Pa s]
η_o	viscosity at ambient conditions [Pa s]
ϑ	coefficient of thermal expansion [dimensionless]
θ	fractional film content [dimensionless]
Θ	lubricant temperature [K]
κ	average asperity density [m^{-2}]
ς	mean asperity tip radius [m]
ρ	density [kg m^{-3}]
ρ_c	density at cavitation pressure [kg m^{-3}]
ρ_o	ambient density of lubricant [kg m^{-3}]
τ	shear stress [Pa]
υ	poisson's ratio [dimensionless]
φ	torsional displacement [rad]
ψ	instantaneous lubricant temperature [°C]

Subscripts

$_{1\cdots7}$	1st to 6th gear pair, 7 refers to reverse gear pair [dimensionless]
$_{brg}$	gear retaining needle bearing [dimensionless]
$_{bp}$	gear pinion base circle [dimensionless]
$_{bw}$	gear wheel base circle [dimensionless]
n',m'	number of simultaneous teeth pairs in mesh [dimensionless]
$_P$	denotes Petrov friction [dimensionless]
$_{pp}$	pinions' pitch location [dimensionless]
$_{pw}$	wheels' pitch location [dimensionless]
$_{PR}$	pinion of the reverse gear [dimensionless]
$_{os}$	output shaft [dimensionless]

Superscripts

$\dot{}$	first time derivative [s^{-1}]
$\ddot{}$	second time derivative [s^{-2}]

Wang and Cheng [10,11] for spur gear pairs have included the effect of boundary interactions as previously described. However, the effect of temperature is significant, requiring a mixed thermo-elastohydrodynamic analysis. Hence, the inclusion of the energy equation is necessary in the aforementioned simultaneous solution of Reynolds and elasticity potential equations. The computational task, therefore, becomes quite arduous. However, it has been shown that in thin film conjunctions heat is conducted away through the bounding solid surfaces, and any convection cooling through lubricant flow may be neglected [12]. This finding provides the opportunity for an analytical solution of the energy equation to obtain the average rise in contact temperature based on viscous shear heating of the lubricant and conduction cooling through the solid boundaries. Gohar and Rahnejat [7] showed the validity of such assumptions for thin elastohydrodynamic films, where a linear temperature gradient across the lubricant film may be assumed. However, one should be cautious that such an analytical solution disregards heat convection from the bounding surfaces at the inlet to the conjunction, which in turn affects the inlet temperature of the lubricant as shown by Olver and Spikes [13]. A simplifying assumption is to consider the inlet temperature to be that of the air–oil mist within the transmission under steady state condition, which itself is assumed to be in thermal equilibrium with the transmission bath of lubricant.

With an assumed Gaussian asperity distribution, only a small area of asperity contact often exists and any temperature rise due to asperity interactions is also deemed to be localised and may thus be neglected, at least in the first instance.

These simplifying assumptions enable the solution of mixed thermo-elastohydrodynamics of gear teeth pair. It should be noted that adoption of such assumptions is crucial under transient conditions, where a number of teeth pair are in simultaneous contact during the gear meshing process as shown by Hua and Khonsari [14].

Whilst the approach expounded here deals with the meshing of a single gear pair, it does not address analysis of modern transmission systems, where a multitude of unselected (unengaged) gear pairs also interact simultaneously. This is as a direct result of a down-sizing trend in transmissions, where pinion teeth impact their loose gear wheel conjungates. The impact/contact loads are light, thus rendering an *improper* meshing of teeth pairs [5,15,16]. These lightly loaded teeth pairs are often treated as being subject to thermo-hydrodynamic regime of lubrication or more crudely as dead band intermittent interactions within the confine of their backlash. The inclusion of loose gear pair interactions is essential in the study of transmission refinement, when dealing with noise and vibration issues such as gear rattle. De la Cruz et al. [5] describe a 7-speed transmission model which

includes an engaged and a number of loose gear pairs, where the engaged teeth pairs are treated under quasi-steady thermo-elastohydrodynamic conditions, using Grubin's extrapolated oil film thickness equation.

The current paper is a tribo-dynamic study of transmission systems, one which combines dynamics of the gear train with tribology of the interacting gear teeth pairs under transient conditions. The engaged (torque transmitting) gear teeth pairs are subject to mixed thermo-elastohydrodynamic regime of lubrication, often subject to non-Newtonian Eyring shear, whereas the loose gear pairs are subject to complex lightly loaded thermo-hydrodynamics in their interacting teeth pairs and Petrov-type friction in loose gear wheel to the retaining shaft conjunctions. This is a comprehensive approach to transmission modelling, not hitherto reported in literature.

2. The tribo-dynamics model

A 7-speed (including reverse gear) transaxle transmission (Fig. 1) is investigated here. It comprises an input shaft, upon which all the pinion gears are mounted. It utilises two output shafts, chiefly in a quest to reduce the required package space. The driven gear wheels are mounted onto these output shafts in the configuration shown in the figure. The study reported here corresponds to an engaged gear pair (transmission in 2nd gear). The backlash between the other unselected gear pairs allows for repetitive impacts of their conjugate teeth pairs. This is fairly common in modern transmissions. The effect of these lightly loaded impacts is a phenomenon commonly referred to as transmission rattle ([5,15,16] among others). This paper is not concerned specifically with the rattle phenomenon, rather the tribological study of various loaded conjunctions, particularly those of engaged (torque transmitting) pairs under a mixed thermo-elastohydrodynamic regime of lubrication. However, dynamics of the system and tribology of various conjunctions are inexorably linked and a realistic tribological assessment necessarily dictates the solution of the tribo-dynamics problem as a whole.

The equations of motion for this transaxle transmission with second gear pair engaged are [5]:

For the 1st gear wheel (unselected):

$$(I_1+I_{PR})\ddot{\varphi}_1 = \sum_{j=1,n'} W_{1,j}r_{bw1} - \sum_{k=1,m'} W_{7,k}r_{bw7} - \sum_{j=1,n'} F_{1,j}r_{x1,j} - \sum_{k=1,m'} F_{7,k}r_{x7,k} - F_{P1}r_{brg1} \quad (1)$$

For the 2nd gear wheel, selected (engaged) pair:

$$(I_2+I_{os})\ddot{\varphi}_2 = \sum_{k=1,n'} W_{2,k}r_{bw2} - \sum_{i=1,3,4,7} \sum_{j=1,n} F_{i,j}r_{xi,j} - \sum_{k=1,n'} F_{2,k}r_{x2,k} - T_{D2} \quad (2)$$

And for the loose unselected pinion-wheel pairs; $i \in 3-6$:

$$I_i\ddot{\varphi}_i = \sum_{j=1,n'} W_{i,j}r_{bwi} - \sum_{j=1,n'} F_{i,j}r_{xi,j} - F_{Pi}r_{brgi} \quad (3)$$

For the reverse gear wheel, denoted by $i=7$; an unselected pair:

$$I_7\ddot{\varphi}_7 = \sum_{k=1,m'} W_{7,k}r_{bw7} - \sum_{k=1,m'} F_{7,k}r_{x7,k} - F_{P7}r_{brg7} \quad (4)$$

For the relatively low torque transferred during creep rattle conditions, the effect of the translational motion on the system's dynamics has been shown to be negligible [17]. Therefore, these additional degrees of freedom were omitted in the current paper, lowering the unnecessary computation time.

The contact forces and the conjunctional frictions are, therefore, necessary to determine the overall dynamic response. In turn, the dynamics of meshing is essential to predict the prevailing tribological performance of various conjunctions. The former is an essential requirement for noise and vibration refinement of a transmission system, whilst the latter determines transmission efficiency and emission characteristics. These attributes can often lead to a contradiction, and a degree of technical pragmatism should normally be exercised.

2.1. Lubricated conjunctions

There are a number of lubricated conjunctions in a transmission system. One can classify these into three types:

(a) Loaded counterformal contact of teeth pairs of the engaged pinion-gear wheel (in the current example; the 2nd gear): these are the meshing gear teeth, with a number of pairs involved simultaneously with different load shares. In the current example 1–2 such teeth pairs are in simultaneous mesh. These conjunctions are subject to moderate to high loads. The lubricant film thickness is fairly thin, thus a mixed thermo-elastohydrodynamic regime of lubrication would usually be expected. One can refer to this class of gear teeth contacts within a transmission system as the engaged gear pairs.

(b) Lightly loaded counterformal contact of gear teeth of unselected pairs: these teeth are in *unintended* (improper) mesh, due to their proximate locations and their repetitive impacts. Light loads and relatively thick films can result in thermo-hydrodynamic regime of lubrication.

(c) Lightly loaded conformal contact of loose wheels, rolling and sliding upon their retaining shafts: the gear wheels are usually mounted upon linear or full complement needle bearings. The conjunction may be regarded as a Petrov bearing with zero eccentricity (unity Petrov multiplier).

The conjunction types (b) and (c) may be referred to as the loose gear pairs.

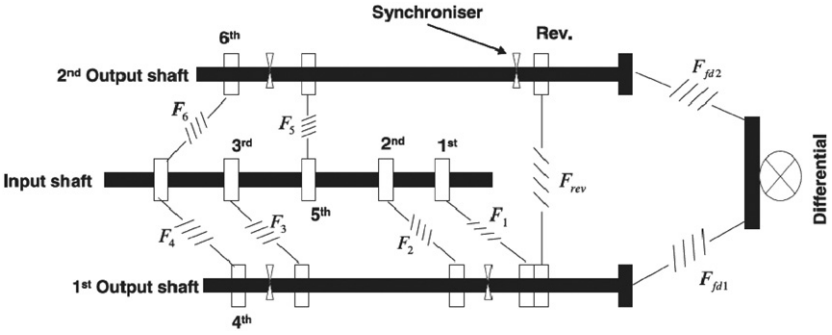

Fig. 1. A 7-speed transaxle transmission.

2.1.1. The engaged gear pair

The teeth pair contacts of the engaged gears are subject to moderate to high loads. For the transmission system studied here, at any instant of time there are 1–2 teeth pairs in simultaneous mesh. These contacting pairs experience engine loading, transmitted through the conjugate engaged pinion, as well as the resistive load torque of the road-wheels and the drive train system. Therefore, unlike the loose gear pairs, the lubricated contacts here encounter an elastohydrodynamic regime of lubrication. The film thickness is usually quite thin. This is because the heat generated because of friction reduces the lubricant viscosity and causes shear thinning of the film. In fact, often asperity interactions take place. Thus, a mixed thermo-elastohydrodynamic regime of lubrication is prevalent. At high loads, significant sliding motion and an insufficient supply of lubricant (modern transmissions have a low depth of oil bath) cavitation can also play a role, resulting in reduced load carrying capacity and paradoxically reduced friction.

Under transient conditions the contact load for any teeth pair conjunction is the integrated pressure distribution. The helical gears of the transmission yield an elastic line contact footprint, which may be assumed to be a thin rectangular strip. Thus:

$$W = \int_{x_i}^{x_e} p dx \tag{5}$$

where, as an initial guess the inlet position x_i may be assumed to be far ahead of the centre of the contact (fully flooded condition). Determination of the position of film rupture, x_e is important in the calculation of contact load. A realistic exit boundary condition, taking into account the effect of cavitation is proposed by Elrod [18].

The contact footprint between the meshing teeth pairs of helical gears is elliptical with large aspect ratio on the account of the equivalent radius on the plane zy (R_y) in Fig. 2(a) being very large compared to that in the plane zx (r_x). Typically, the aspect ratio$=R_y/r_x > 10$. In fact, at the beginning of a mesh this ratio is

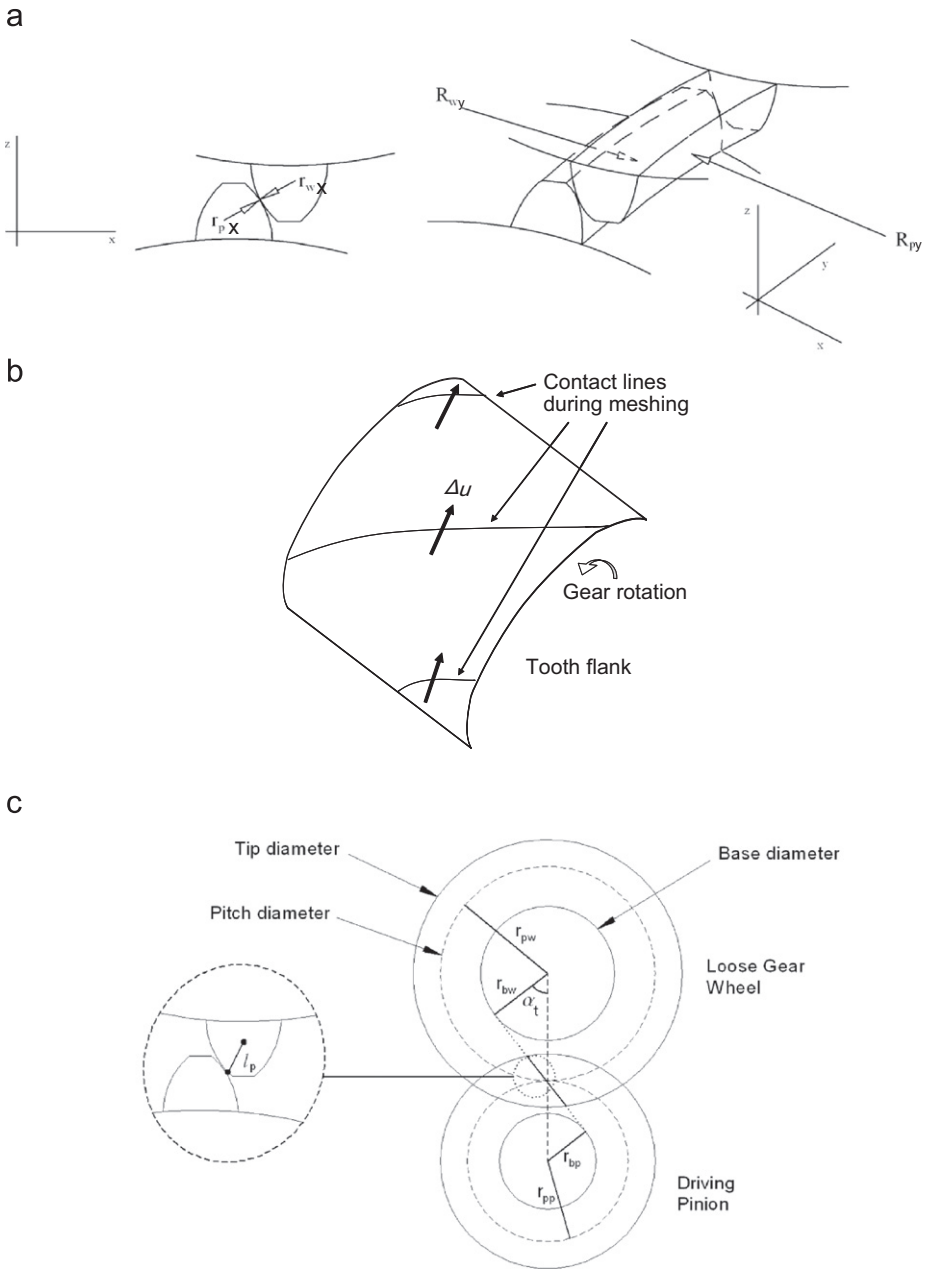

Fig. 2. Gear meshing sequence.

40, at the maximum load it is 41 and at the end of mesh it just exceeds 10. Therefore, it is reasonable to assume a long line contact, for which Reynolds' equation becomes:

$$\frac{\partial}{\partial x}\left[\frac{\rho h^3}{\eta}.\frac{\partial p}{\partial x}\right]=12\left\{u_{av}\frac{\partial}{\partial x}(\rho h)+\frac{d}{dt}(\rho h)\right\} \tag{6}$$

where, the speed of entraining motion of the lubricant into the contact is:

$$u_{av}=\frac{1}{2}(u_p+u_w).$$

Note that the corresponding sliding velocities (u_p,u_w):

$$u_p=v_{pitch}\left(\sin\alpha_t+\frac{l_p}{r_{pp}}\right)\cos\beta_b,\ u_w=v_{pitch}\left(\sin\alpha_t-\frac{l_p}{r_{pw}}\right)\cos\beta_b \tag{7}$$

The assumption of a line contact has the drawback of ignoring side leakage from the contact. However, this is accounted for by the angled flow calculation of surface velocities in Eq. (7) which are perpendicular to the line of contact at any instant of time by transformations through helix and tangential pressure angles (Fig. 2(b)).

The non-holonomic constraint function at the pitch point determines the pitch velocities as: $v_{pitch}=r_{pp}\dot{\phi}_p=r_{pw}\dot{\phi}_i$ for $i=1-7$. Also: $l_p=r_{pw}\sin\alpha_t-r_{wx}$ (Fig. 2(c)).

If the instantaneous radii of curvature of a pinion gear tooth and its conjugate gear wheel tooth are r_{px} and r_{wx}, respectively, then the reduced radius of the concentrated counterformal contact (that of an equivalent ellipsoidal rigid solid against a semi-infinite elastic half-space) is: $r_x=r_{px}r_{wx}/(r_{px}+r_{wx})$, and the reduced elastic modulus of the semi-infinite solid under plane strain condition is: $E'=E/(1-\upsilon^2)$ where: $E_p=E_w=E$ and $\upsilon_p=\upsilon_w=\upsilon$.

The form of Reynolds' equation stated above assumes the formation of a coherent lubricant film in the conjunction, prior to a film rupture point. The generated pressures fall below the vapour pressure of the lubricant in the region of contact exit (with cavitation taking place). This can reduce the load carrying capacity of the contact, as well as affect the underlying mechanisms that contribute to friction. It is, therefore, more instructive to account for this effect. A solution to this problem was first obtained by considering a full film region, followed by a cavitated region and film reformation beyond it by Jakobsson and Floberg [19] and Olsson [20], who assumed a set of exit boundary conditions, which has come to be known as the JFO boundary conditions. On the other hand, Reynolds' equation in the form stated above is suited to the region of full film, and is often used in conjunction with the Swift–Stieber boundary conditions, which determine the oil film rupture position, x_e. The solution does not extend beyond this point, where continuity of flow conditions, based only on the Couette flow has to be satisfied. An approximate solution to the rather computationally intensive approach of Jakobsson and Floberg [19] and Olsson [20] was first proposed by Elrod [18], which is based on a fractional film content θ, where any value equating unity or in its excess implies the presence of a coherent lubricant film (this being a film sustained above the vaporisation cavitation pressure of the lubricant). Consequently, a value of $0<\theta<1$ suggests the presence of vapour bubbles within a film of lubricant. Hence:

$$p=g\beta\ln\theta+p_c \tag{8}$$

where g may be regarded as a switching function: $g=1,\ \theta\geq 1$ (Full film) and $g=0,\ 0<\theta<1$ (partial film: cavitation). Reynolds' equation can now be rewritten in terms of θ as:

$$\frac{\partial}{\partial x}\left[\frac{\rho h^3}{\eta}g\beta\frac{\partial\theta}{\partial x}\right]=12\left\{u_{av}\frac{\partial}{\partial x}(\rho\theta h)+\frac{\partial}{\partial t}(\rho\theta h)\right\} \tag{9}$$

It can be seen that in the cavitated region the flow takes place due to Couette flow only (on the right hand side of the equation), as well as film *memory* represented by squeeze film effect (the ultimate term on the right hand side of the equation). Clearly, under this condition, $\rho=\rho_c$ at $p=p_c$. Hence:

$$\left\{u_{av}\frac{\partial}{\partial x}+\frac{\partial}{\partial t}\right\}(\rho_c\theta h)=0 \tag{10}$$

The elastic film shape is:

$$h=h_0+h_s+\delta \tag{11}$$

The localised contact deflection is obtained by solution of elasticity potential equation [7]. For an elastic line contact this simplifies to:

$$\delta_m=\frac{1}{\pi E'}\int\frac{p_k}{(x_m-x_k)}dx_k \tag{12}$$

where, the deflection at a point x_m results from all the generated pressures at points x_k. When a one dimensional computational grid is made with the pressure distribution, p_k, this equation can be stated as:

$$\delta_m=\sum_k D_m^k p_k \tag{13}$$

where, δ_m is the vector of contact deflections and D_m^k contains the influence coefficients (see Appendix A1).

Now, simultaneous solution of Eqs. (9) or (10) for full film or cavitation region with (11) and (13) yields values of p, δ, h and θ for an isothermal iso-viscous analysis. However, it is important to take into account the effect of lubricant rheological state (ρ,η).

Lubricant density is adjusted for pressure [2]:

$$\overline{\rho}=\frac{\rho}{\rho_o}=1+\frac{0.6\times10^{-9}p}{1+1.7\times10^{-9}p} \tag{14}$$

Any significant change in lubricant density will be noted in the cavitation region. In the region of full film, under elastohydrodynamic conditions, the lubricant is almost incompressible. The main lubricant rheological change is its viscosity under the prevalent thermo-elastohydrodynamic conditions. The lubricant viscosity is, therefore, adjusted using Houpert's [21] equation, which assumes Newtonian behaviour of the lubricant:

$$\eta=\eta_o e^{\alpha^* p} \tag{15}$$

where:

$$\alpha^*=\frac{1}{p}[\ln(\eta_o)+9.67]\left\{\left(\frac{\Theta-138}{\Theta_o-138}\right)^{-s_0}\left[\left(1+\frac{p}{1.98\times10^8}\right)^Z-1\right]\right\} \tag{16}$$

Note, Θ is temperature in $^\circ K$, thus: $\Theta=\psi+273$.

$$\text{Also}:\ Z=\frac{\alpha_o}{5.1\times10^{-9}[\ln(\eta_o)+9.67]}\text{and}\ s_0=\frac{\beta'(\Theta_o-138)}{\ln(\eta_o)+9.67}$$

The elastohydrodynamic conjunctions of loaded gear teeth pairs are subject to contact kinematics which undergoes rolling, sliding and normal approach and separation (squeeze film action). The sliding motion, in particular, causes viscous shear of the lubricant which results in a corresponding rise in its temperature. This, in turn affects the lubricant viscosity. In order to account for this, the solution to the above set of equations should be accompanied by the energy equation:

$$\vartheta u_{av}\psi\frac{\partial p}{\partial x}+\eta\left(\frac{\partial u_{av}}{\partial z}\right)^2=\rho u_{av}C_p\frac{\partial\psi}{\partial x}-k\frac{\partial^2\psi}{\partial z^2} \tag{17}$$

For a thin rectangular contact footprint, as in a concentrated elastic line contact with a thin elastohydrodynamic film, Gohar and Rahnejat [7] show that an order of magnitude analysis

indicates the dominance of conduction cooling, thus the penultimate term in the above equation, being due to convection cooling may be neglected. The contrary is true for loose gear teeth pairs, where lightly loaded hydrodynamic conditions dominate, as described in Section 2.2.2. If viscous shear heating (the second term in (17)) is assumed to dominate the heating of the lubricant (at high shear), then the energy equation simplifies by ignoring the first term due to compressive heating. Assuming that the temperature rises linearly across the film (with one surface assumed stationary and the other moving with relative velocity, Δu), then the average temperature rise of the lubricant within the hydrodynamic contact becomes [5]:

$$\Delta\psi = \frac{4b\eta\Delta u}{h^2\rho C_p} \tag{18}$$

where, the sliding velocity is: $\Delta u = u_p - u_w$.

Using the principle of superposition to also account for compressive heating (EHL), the average temperature rise in a narrow rectangular contact footprint was obtained by Karthikeyan et al. [22] as:

$$\Delta\psi = \left\{\frac{\vartheta u_{av}\psi_i hp_m + (2b\eta\Delta u^2/h)}{(bk/h) - \vartheta u_{av} hp_m}\right\} \tag{19}$$

where $\psi = \psi_i + \Delta\psi$ is the average lubricant temperature in the contact for an inlet temperature of ψ_i. p_m is the mean pressure peak in an elastohydrodynamic pressure distribution which is in fact, for all intent and purposes, the Hertzian mean pressure. Thus, the half-width of the rectangular contact strip, b may be obtained from the classical Hertzian theory as: $b = 2(Wr_x/\pi\ell E')^{1/2}$, where ℓ is the contact length [16]. Appendix A2 shows typical contact length variation for a teeth pair through mesh.

Now the effective lubricant viscosity can be obtained from Eq. (15), and the simultaneous solution of this equation with (9) or (10), (11), (13) and (14) yields the pressure distribution and the corresponding film thickness, usually sought in tribological studies.

The simple analytical method used here to calculate the rise in the contact temperature disregards the temperature rise caused by any asperity interactions. It is assumed that a small proportion of the real contact area accounts for asperity contact and the nature of generated heat is localised, mainly leading to plastic deformation of asperity pairs. It should also be noted that the analytical method provides the average temperature rise in the contact, thus localised effects play a small role.

To solve Eq. (2), flank friction terms $F_{i,k}$, $i = 2$ (engaged gear pair) and $k \in 1,2$(number of teeth pairs in simultaneous contact) are required. Thermo-elastohydrodynamic films, h, may be of insufficient thickness to guard against asperity interactions on the contiguous surfaces. Therefore, the overall flank friction is given as a combination of viscous friction, F_v and boundary, F_b interactions as: $F = F_v + F_b$. These individual contributions are determined according to the lubricant shear stress,

$$\tau = \pm\frac{h}{2}\frac{dp}{dx} + \frac{\eta\Delta u}{h}$$

If $\tau < \tau_0$, being the Eyring shear stress [6], then:

$$F_v = \tau(A - A_e) \tag{20}$$

where, the Eyring shear stress for the transmission fluid used is 4.5 MPa, and A_e is the real contact area, as opposed to the apparent contact area, determined by the Hertzian theory, A [8]:

$$A_e = \pi^2(\varsigma\kappa\sigma)^2 AF_2(\lambda) \tag{21}$$

where, $A = 2\ell b$. $\lambda = h/\sigma$ is the Stribeck [23] oil film parameter, with σ being the composite root mean square roughness of the contiguous surfaces in contact.

If, on the other hand, $\tau \geq \tau_0$, then the shear stress is adjusted to: $\tau = \tau_0 + \gamma p^*$, where:

$$p^* = \frac{W - W_e}{A_e} \tag{22}$$

with W given by Eq. (5) and the load share of asperities (W_e) is obtained as [7,8]:

$$W_e = \frac{8\sqrt{2}}{15}\pi(\varsigma\kappa\sigma)^2\sqrt{\frac{\sigma}{\kappa}}E' AF_{5/2}(\lambda) \tag{23}$$

The variables F_2 and $F_{5/2}$ are statistical functions introduced to match the assumed Gaussian distribution of asperities considered. Teodorescu et al. [24,25] propose a polynomial fit to describe these functions (Fig. 3). Now the boundary contribution to friction is obtained as:

$$F_b = \tau_0 A_e + \xi W_e \tag{24}$$

where ξ is the pressure coefficient for boundary shear strength for direct asperity interactions of ground heat treated high alloy steel, approximated to 0.17 for this study [5,25].

The analysis for the simulated conditions pertaining to transmission creep rattle (transmission engaged in 2nd gear with engine in the speed range 800–2000 rpm) has shown that lubricant shear

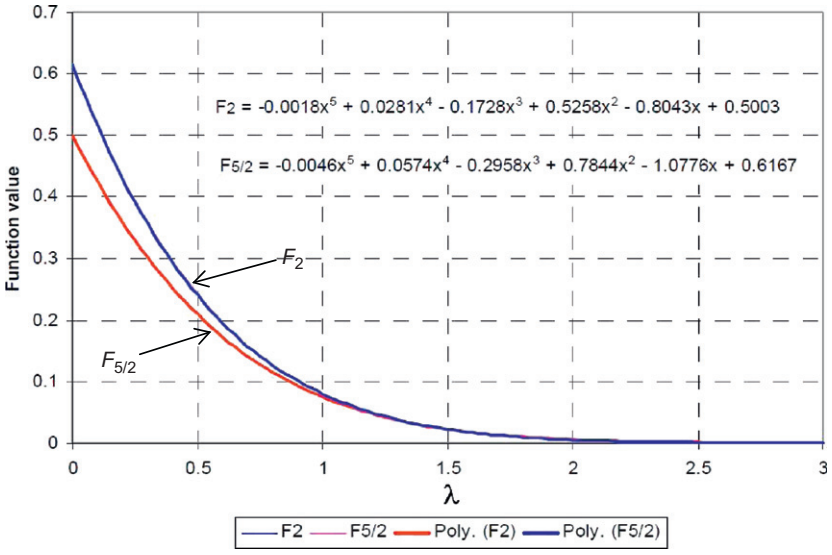

Fig. 3. 5th order fit for the statistical functions (after Teodorescu et al., 2007).

stress remains always below its Eyring stress limit. At higher engine speeds and applied torques this may not be always true. Therefore, for sake of generality the entire process described above is retained.

The total contact load between any pair of meshing teeth in the engaged gear pair is a combination of load carried by the elastohydrodynamic lubricant film and the share of load carried by the asperity pairs, thus: $W_{2,k}=W_e+\int p dx$, $k\in 1-n$, n being the number of teeth in simultaneous contact at any given time. This is used in Eq. (2) for simultaneous pairs of teeth in contact; k. It is clear that as meshing of a pair of teeth progresses, the principal radii of curvature at the point of contact change, which in turn alters the speed of entraining motion, film thickness and pressure distribution. Consequently, the contact load alters (i.e. $W_{2,k}$,$k\in 1-n$ are functions of the meshing cycle/time). The stiffness of each teeth pair contact is a function of the rate of change of load during meshing. This is implicit in Eq. (2). Similarly, damping may be regarded as the rate of change of flank friction during meshing for all simultaneous teeth pairs. It dissipates the vibratory energy. For elastohydrodynamic contact of gears damping is found to be quite low, although included in Eq. (2) in terms of flank friction. Other sources of damping due to support bearings or bearing housing are ignored in the current analysis.

2.1.2. The loose gear pair

As noted in Section 2.1 there are two types of conjunctions in the loose gear pairs' interactions. These are the teeth pair flank contacts and those for loose wheels-to-their retaining output shafts. For the counterformal contact of the former an analytical one dimensional solution to Reynolds' Eq. (6) can be obtained with no side-leakage and use of half-Sommerfeld boundary conditions [26,27]. Therefore, the integrated pressure distribution for any pair of lightly loaded teeth, rolling with squeeze film effect is obtained as the lubricant reaction according to Eq. (5) as:

$$W=\frac{2\ell u_{av}\eta r_x}{h}-\frac{3\pi\ell\eta}{\sqrt{2}}\left(\frac{r_x}{h}\right)^{3/2}\frac{\partial h}{\partial t} \tag{25}$$

where the squeeze film velocity is obtained as a first order approximation by $\partial h/\partial t=(h_i-h_{i-1})/\Delta t$, where the film thickness change corresponds to two successive simulation time steps. Note that when $\partial h/\partial t<0$, the bounding surfaces approach each other, resulting in an enhanced load carrying capacity (Eq. (25)). On the contrary, when $\partial h/\partial t>0$, separation occurs, and the second term in Eq. (25) is omitted.

For the iso-viscous rigid conditions assumed here, the lubricant film thickness is as the result of the difference in the nominal clearance of the teeth pairs and their mutual approach, thus:

$$h=\begin{cases} C-\frac{r_{bpi}\varphi_p-r_{bwi}\varphi_i}{\cos\alpha_n\cos\beta_b}, & r_{bpi}\varphi_p>r_{bwi}\varphi_i \\ C+\frac{r_{bpi}\varphi_p-r_{bwi}\varphi_i}{\cos\alpha_n\cos\beta_b}, & r_{bpi}\varphi_p<r_{bwi}\varphi_i \end{cases} i\in 1\to 7\notin 2 \tag{26}$$

Note that the motion of all the pinions are specified by the transmission input shaft (i.e. φ_p is known *a priori*). This motion is obtained experimentally and is an input to the simulation study. It is a function of engine speed and all its harmonics, known as engine orders [28]. For an assumed thin rectangular footprint of length ℓ, the flank friction is obtained as [29]:

$$F=\begin{cases} \frac{\ell\pi\eta\Delta u}{\sqrt{2h}}\sqrt{r_x}, & \text{when} \quad \Delta u\geq 0 \\ \frac{-\ell\pi\eta\Delta u}{\sqrt{2h}}\sqrt{r_x}, & \text{when} \quad \Delta u<0 \end{cases} \tag{27}$$

The loose gear wheels, when impacted upon, rotate relative to their supporting shaft. As already noted, these conjunctions are treated as Petrov bearings, thus [5]:

$$F_P=\frac{2\pi\eta u_{brg}r_{brg}l_{brg}}{c} \tag{28}$$

where, the speed of lubricant entrainment is given as: $u_{brg}=1/2(r_{brg}\dot{\varphi}_i+(1/2\pi)r_{os}\dot{\varphi}_{os})$ $i\in 1-7,\notin 2$.

For both loose gear pair conjunctions analytical solutions to the energy Eq. (17) are obtained. In the case of teeth flanks, lubricant heating is assumed to be as the result of viscous shear, with negligible compressive heating, whilst the heat is taken away from such conjunctions by convection cooling due to relatively thick films of at least several micrometres. A linear temperature distribution is assumed along the rectangular strip footprint of width $2b$ as: $\partial\psi/\partial x=\Delta\psi/2b$. Implementing these assumptions into the energy Eq. (17) and after integration:

$$\Delta\psi=\frac{8\eta b\Delta u}{h^2\rho C_p} \tag{29}$$

The film thickness values in the loose gear pair are quite large; of the order of several to tens of micrometres. The average temperature rise is very small and there is no localised rise due to any asperity interactions (the Ra value for these particular gears is 0.4 μm).

The Petrov conjunctions are essentially journal bearings with zero eccentricity (unity Petrov multiplier). For relatively thick hydrodynamic films, one can employ the procedure developed for journal bearings by [7] to obtain the temperature rise as:

$$\Delta\psi=\left(\frac{2K_1W_{brg}}{\rho C_p r_{brg}l_{brg}}\right)\left(\frac{\mu^*}{Q_s^*}\right) \tag{30}$$

where

$$\mu^*=\frac{\pi\eta u_{brg}l_{brg}}{W_{brg}}\left(\frac{r_{brg}}{c}\right)^2 \text{ and } Q_s^*=\frac{Q_s}{\pi N r_{brg}l_{brg}c}=2\varepsilon$$

and the coefficient K_1 admits that not all the frictional power is lost through convection.

The temperature rise is then used to obtain the effective viscosity of the lubricant in the same manner as in the case of loaded gear teeth pairs.

Loose gear pairs are lightly loaded. The effective stiffness of teeth pair contacts can be obtained as the rate of change of instantaneous hydrodynamic reaction with respect to the hydrodynamic film thickness; $k=\partial W/\partial h$. Clearly, as in the case of the engaged gear this is a function of the meshing properties. The effective damping is a function of squeeze film action; $c=\partial W/\partial\dot{h}$, where: $\dot{h}=\partial h/\partial t$. Flank friction and Petrov friction, described above also contribute to damping. These effects are already included in the equations of motion for $i=1-7,\notin 2$.

3. Method of solution

The solution method used is low relaxation effective influence Newton–Raphson (EIN) method with Gauss–Seidel iterations for the thermo-elastohydrodynamic conjunctions at each step of time (Jalali-Vahid et al. [30] for point contacts and Teodorescu et al. [31] for line contact and Chong et al. [32] for line contact with cavitation boundary). The equations of motion are solved using the linear acceleration method, described by Newmark [33] and Timoshenko et al. [34] with the adoption method for the case of lubricated contacts, outlined by Rahnejat [27]. The overall procedure is highlighted by Gohar and Rahnejat [7].

For the sake of numerical stability the governing equations for lubricated contacts are non-dimensionalised. Thus, Reynolds' Eq. (9) with Elrod modification becomes (see Appendix A3 for non-dimensional variables):

$$\frac{\partial}{\partial X}\left[\frac{\overline{\rho}H^3}{\overline{\eta}}\frac{\partial}{\partial X}g(\theta-1)\right]=\Upsilon\left\{\frac{\partial}{\partial X}(\theta\overline{\rho}H)+\frac{r_x}{b}S\overline{\rho}\theta\right\} \tag{31}$$

where, $S=(1/u_{av})(\partial h/\partial t)$ is the squeeze-roll ratio and

$$\Upsilon=\frac{12\eta_0 u_{av}}{\beta b}\left(\frac{r_x}{b}\right)^2, \text{ also } g\frac{d\theta}{dX}=\frac{dg(\theta-1)}{dX}$$

which retains the physical meaning of Eq. (8) [35] in the subsequent use of finite differences.

$$H=H_0+H_s+\Delta \tag{32}$$

where, the non-dimensional form of deflection is:

$$\Delta=D(X)\frac{g\beta(\theta-1)+p_c}{p_H} \tag{33}$$

Now the above equations are put in finite difference form (Appendix A3) and solved in each step of time during simulation in the form:

$$\sum_{k=1}^{n-1} J_m^k \Delta\theta_k=-\overline{F}_m^R \tag{34}$$

where J_m^k and $\overline{F}_m^R$ are the Jacobian and residual terms, respectively.

There are two convergence criteria. One is for the computation of fraction film content (Gauss–Seidel iterations):

$$\frac{\sum_m|\theta_m^k-\theta_m^{k-1}|}{\sum_m\theta_m^k}\le\varepsilon_\theta \tag{35}$$

where, typically: $2.5\times10^{-7}\le\varepsilon_\theta\le3.5\times10^{-7}$.

If the above criterion is not satisfied, then under-relaxation is used in the form:

$$(g\theta)_m^k=(g\theta)_m^{k-1}+\Omega\Delta\theta_m^k \tag{36}$$

where, the under-relaxation factor is typically $\Omega=5\times10^{-5}$.

The other convergence criterion is for system dynamics based on the Newmark's linear acceleration method:

$$\left|\frac{\ddot{\varphi}_l^j-\ddot{\varphi}_l^{j-1}}{\ddot{\varphi}_l^j}\right|\times100\le0.01 \text{ for } l\in1-7 \tag{37}$$

Here l refers to a gear pair. If the criterion is not met, then the conjunctional gaps (rigid separations) are adjusted as:

$$H_0^k=H_0^{k-1}\left(\frac{W^k}{W^{k-1}}\right)^{\varsigma} \tag{38}$$

where, the damping factor is typically: $\varsigma=0.05$.

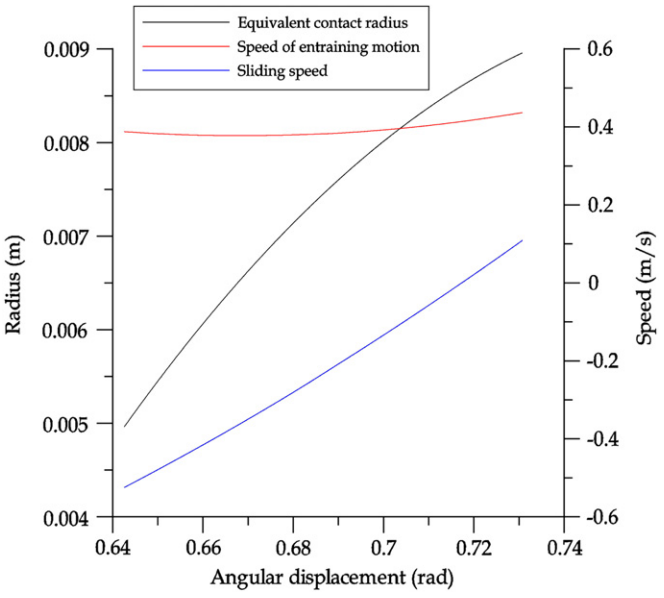

Fig. 4. Variation of contact geometry and kinematics.

4. Results and discussion

A number of simulation studies of the entire transmission model are reported here for the bulk oil temperatures of 50 °C and 60 °C, respectively. Note that the inlet oil temperature is assumed to be that of the bath of oil. All simulation studies are for the case of 2nd gear pair selected and after the initial transient response has elapsed. The time-step of simulation in all cases is set to 1 μs. The spatial discretisation for the solution of Reynolds' equation is based on 500 elements in the direction of entraining motion. All the problem data are provided in Appendix A4.

Fig. 4 shows the equivalent reduced radius of contact of any meshing teeth pair of the 2nd gear set. The abscissa in the figure refers to the angular position of the gear wheel in a typical meshing cycle. The position of the pitch point is at $\varphi_w=$ 0.714 rad. At this point the contact is subject to pure rolling

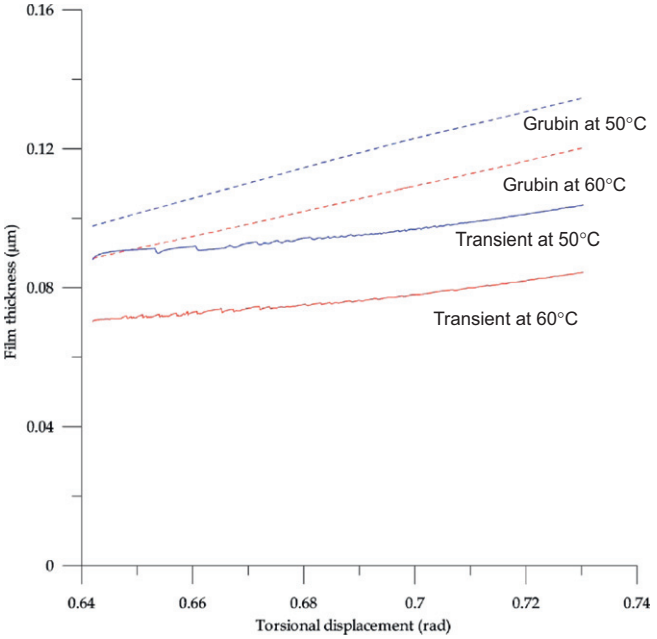

Fig. 5. Transient history of central oil film thickness of typical loaded gear teeth pair.

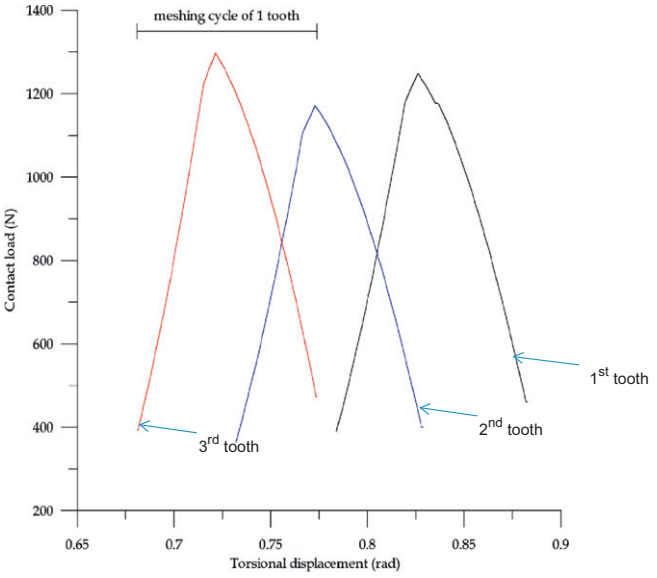

Fig. 6. Teeth pair load share through mesh (transient at 60 °C).

motion (no sliding). The speed of entraining motion changes only marginally through mesh. This means that the film thickness changes only slightly through mesh (being mainly dependent on the speed of entraining motion under EHL conditions, Fig. 5). However, the shear stress τ alters due to the sliding speed, away from the pitch point (sliding speed changes direction). This is the main cause of viscous friction and generated heat, thus altering the effective lubricant viscosity. Hence, the results are for the transient mixed thermo-elastohydrodynamic analysis of the 2nd gear teeth contacting pairs through mesh.

Fig. 5 shows the predicted central oil film thickness at 50 °C and 60 °C inlet bulk oil temperatures respectively. It can be seen that with the increased inlet temperature, the lubricant film has reduced by nearly 15%. The results also show that the film is significantly thinner than the root mean square roughness of the contiguous surfaces in contact, being 0.5 μm. At best, this points to a mixed regime of lubrication. The corresponding load variation through a meshing cycle for the transient analysis is shown in Fig. 6, indicating the load shared per teeth pair contact during meshing. As noted previously between 1 and 2 teeth pairs are in simultaneous mesh. Taking into account Figs. 5 and 6 together, the important observation is that the lubricant film thickness remains almost insensitive to load, which is indicative of prevailing elastohydrodynamic conditions.

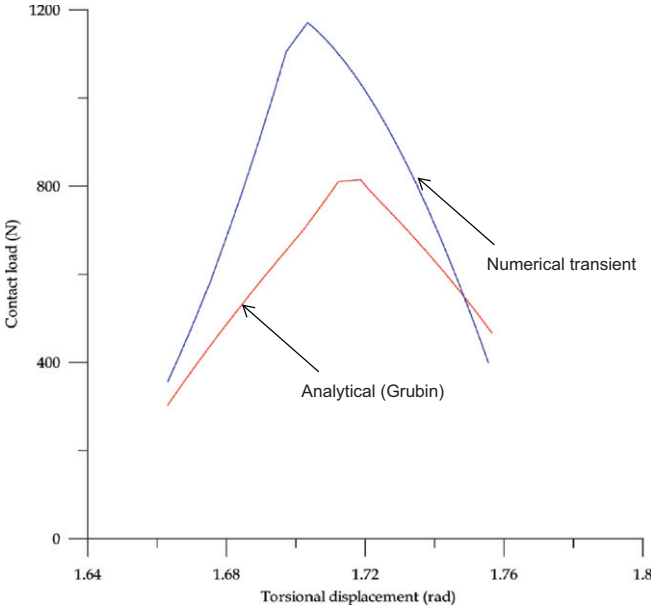

Fig. 7. Comparison of load per EHL conjunction under transient and analytical quasi-static conditions (transient at 60 °C).

Fig. 5 also includes the film thickness predicted for the same bulk oil temperatures using a quasi-static solution, based on the lubricant film thickness equation of Grubin [1] with adjustment made for viscosity variation with temperature [5]. There is reasonable agreement considering that the results of quasi-static (analytical Grubin) solution correspond to a lubricant reaction around 20–30% lower than the current transient analysis (Fig. 7). This shows that a higher load carrying capacity is achieved under transient conditions because of the contribution from squeeze film action. One conclusion from this comparison is that the use of much simpler quasi-static analysis may be regarded as a reasonable first approximation with a considerably reduced computation time (a few CPU seconds for analytical solution versus several hours for the transient analysis).

As can be observed in Fig. 6, the contact load (lubricant reaction) rises by threefold in any teeth pair contact during mesh. Fig. 8 shows a series of EHL pressure distributions with their corresponding elastic film shapes. These locations are for instants of contact of a meshing teeth pair, prior to, at, and after the pitch point.

The contact conditions remain within EHL (viscous–elastic) at all times. This is shown in the Greenwood chart (Fig. 9) for regimes of fluid film lubrication. The predicted conditions in Fig. 8 are depicted on the chart (a–d). The points indicated by a' and b' on the chart are typical conditions related to a pair of meshing teeth of the 5th loose gear set. These are subject to the lightly loaded iso-viscous rigid (hydrodynamic) regime of lubrication.

To observe rattle conditions as is usually perceived in accord with high level of annoyance, double-sided teeth impact in loose gears should be promoted. In practice such conditions are noted for bulk oil temperatures exceeding 70 °C or 80 °C. Fig. 10(a) and (b) for loose gear pairs correspond to the points (a) and (b) on the

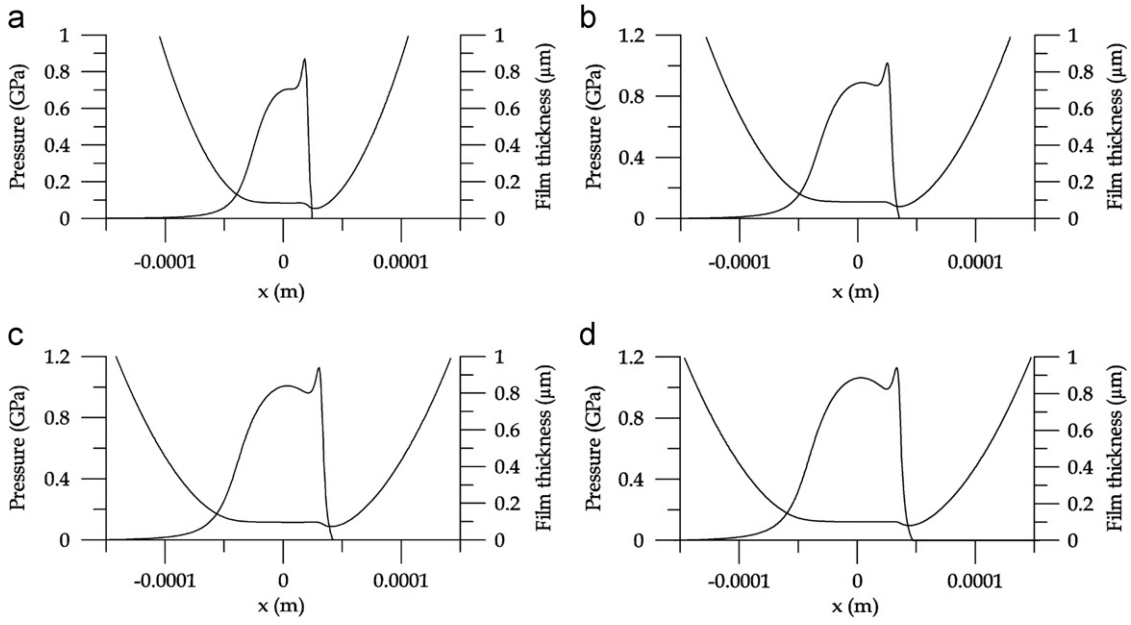

Fig. 8. Pressure distribution and film profile (transient at 60 °C). (a) Beginning of meshing cycle (φ=0.642), (b) highest load point (φ=0.681), (c) pitch point (φ=0.714) and (d) end of meshing cycle (φ=0.734).

Greenwood chart and are for bulk oil temperatures of 20 °C and 80 °C, respectively. It is noted that the film thickness far exceeds that predicted for any engaged gear teeth pair conjunction (by up to 2 orders of magnitude) and fluctuates due to the impacting nature of these lightly loaded conditions. This may be regarded as repetitive mutual approach and separation of teeth pairs, which is exacerbated by the increased bulk lubricant temperature. In the case of Fig. 10(b), the approach and separation of teeth spans the nominal backlash, corresponding to double-sided impact of loose gear teeth pairs. This promotes the conditions commonly perceived and referred to as rattle, described in some detail in De la Cruz et al. [5].

It is clear that larger variations in film thickness in successive contact separation and squeeze effect in the lightly loaded contacts would induce pressure perturbations that contribute to noise propagation from the impact sites. This effect is minimal in loaded elastohydrodynamic conjunctions due to almost constant film thickness through mesh. However, in practice transmission error can induce momentary losses of contact that induce impulsive actions. This is more common in the cases of hypoid gears of differential systems. The resulting emanated noise is referred to as axle whine [36]. Therefore, noise and vibration refinement is mainly governed by the tribo-dynamics of unengaged loose gear pairs. On the contrary, transmission efficiency because of frictional and thermal losses is determined by the interactions of engaged gear pairs. Fig. 11(a) shows the generated friction in the elastohydrodynamic conjunction of a pair of teeth of the engaged 2nd gear pair, whilst its counterpart for a pair of teeth of the loose 5th gear pair is shown in Fig. 11(b). Note the insignificant generated friction in the case of the latter. There is no viscous friction at the pitch point due to instantaneous pure rolling motion of the teeth pair there. The same does not arise in the loaded conjunction, because of high boundary friction at the pitch point.

5. Conclusion

Modern transmission engineering is concerned with efficiency, emission and noise and vibration refinement. Progressively, analysis plays an important and an integral part of design and development. Therefore, models should take all the aforementioned key concerns into account. This constitutes development of multi-speed transmission tribo-dynamic models, rather than the traditional gear pair models. Such a model is described in this

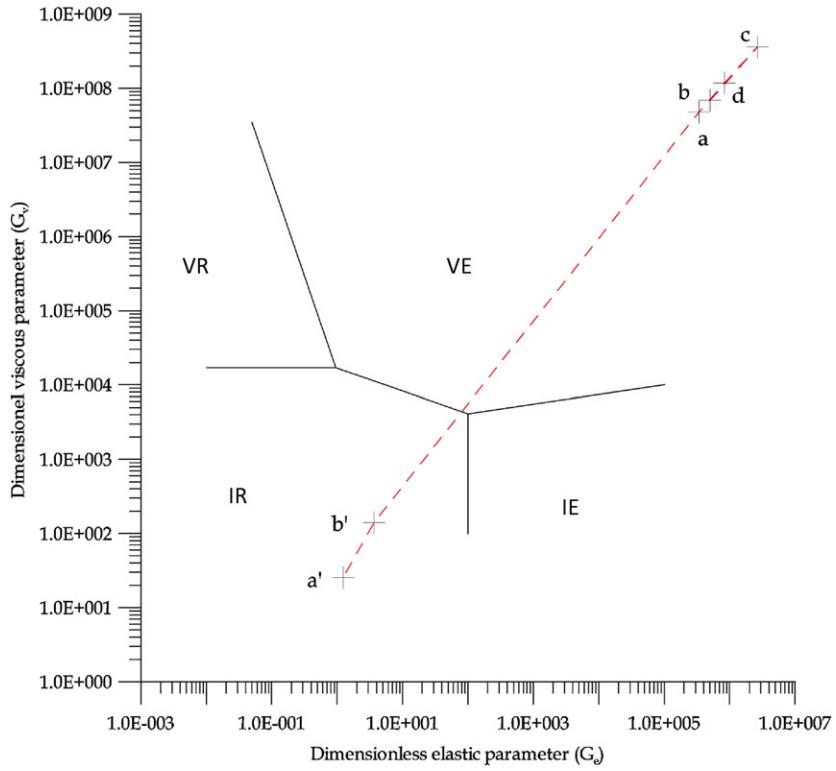

Fig. 9. Greenwood chart ($G_e = W^{*8/3}/U^{*2}$, $G_v = G^*W^{*3}/U^{*2}$, see Appendix A3). IR=Iso-viscous Rigid, IE=Iso-viscous Elastic, VR=Viscous Rigid, VE=Viscous Elastic (EHL).

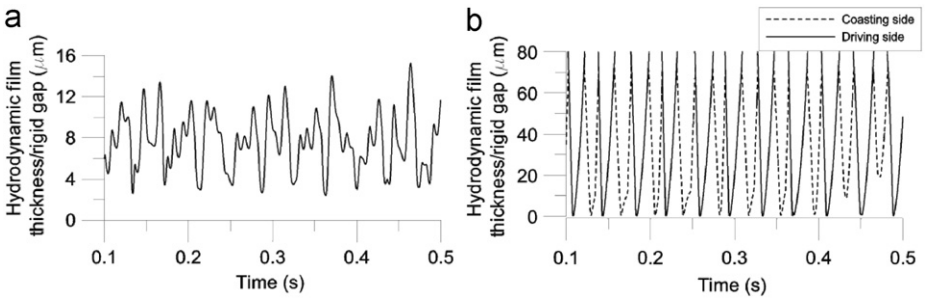

Fig. 10. Fluctuations in film thickness in lightly loaded conjunctions of loose gear pair.

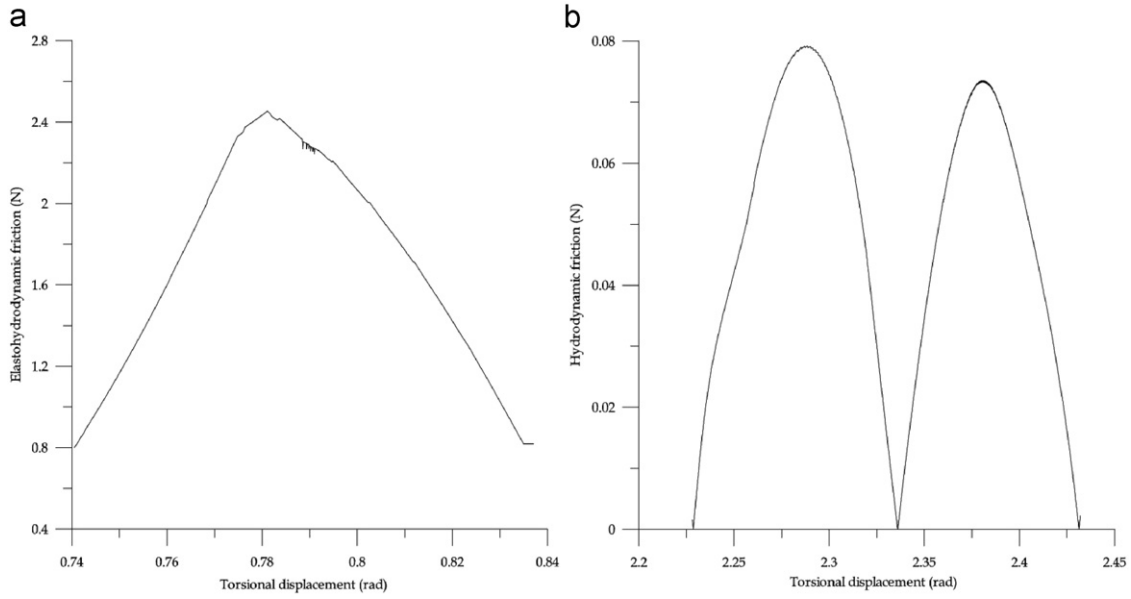

Fig. 11. Friction in loaded and loose gear pair conjunctions through a meshing cycle. (a) Loaded gear teeth pair and (b) unloaded loose gear teeth pair.

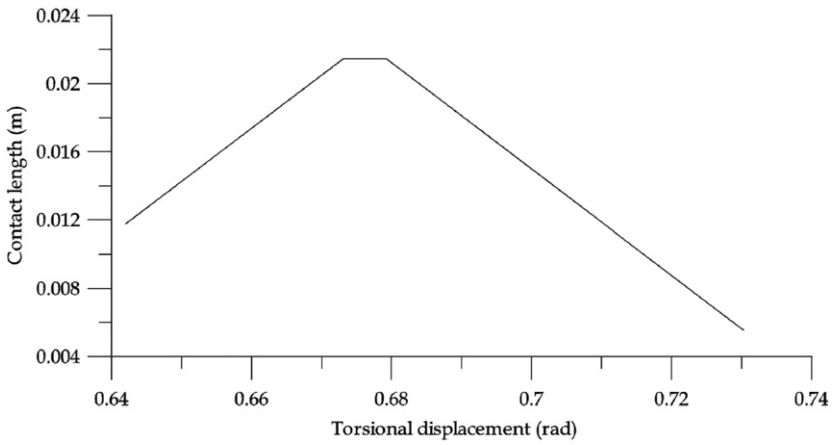

Fig. A2. Variation of thin rectangular strip length in meshing of a gear teeth pair (the instantaneous contact width, b is obtained through Hertzian theory, Section 2.1.1).

paper, comprising transient mixed thermo-elastohydrodynamics of loaded gear teeth pairs as well as thermo-hydrodynamics of loose (unengaged) gear pair conjunctions. The results show that whilst the loose gear pairs are the main sources of noise and vibration response of a transmission, frictional and thermal losses, thus emission characteristics of the transmission are affected by the engaged gear pair conjunctions.

The reported model can be used to study a plethora of noise and vibration concerns as well as assessment of likely palliative actions. It can also be employed to study the effect of tribological parameters on transmission efficiency such as lubricant rheology, surface topography, gear teeth form and transmission error.

Acknowledgments

The authors wish to express their gratitude to the Engineering and Physical Sciences Research Council (EPSRC) for its financial support of the research project: Automotive Transmission Rattle and Ford Motor Company under its University Research Programme (URP). Thanks are also due to other project research partners; Getrag Ford, GKN and AVL.

Appendices

Appendix A1

$$D_{m(i,l)} = -\frac{1}{2\pi}\left(a_3 K + a_4 \frac{M}{2}\right)$$

where :

$$a_3 = \frac{2}{(X_i - X_{i-1})(X_i - X_{i+1})}$$

$$a_4 = -\frac{(X_{i+1} - X_{i-1})}{(X_i - X_{i-1})(X_i - X_{i+1})} + \frac{2}{(X_i - X_{i-1})(X_i - X_{i+1})} X_i$$

$$M = (X_l - X_{i-1})^2(\ln(X_l - X_{i-1})^2 - 3) - (X_i - X_{i+1})^2(\ln(X_l - X_{i+1})^2 - 3)$$

$$N = (X_l - X_{i+1})^3(\ln|X_l - X_{i+1}|^3 - 4) - (X_l - X_{i-1})^3(\ln|X_l - X_{i+1}|^3 - 4)$$

$$K = M\frac{X_l - X_i}{2} + \frac{2N}{9}$$

Appendix A2

The length of the elastic line contact footprint along the flank of a pair of meshing teeth is shown in Fig. A2 below.

Appendix A3

The non-dimensional terms are:

Parameters	Dimensionless form	Expression
$x(m)$	X	$X=\frac{x}{b}$
$\rho(kg/m^3)$	$\overline{\rho}$	$\overline{\rho}=\frac{\rho}{\rho_o}$
$\eta(Ns/m^2)$	$\overline{\eta}$	$\overline{\eta}=\frac{\eta}{\eta_o}$
$h(m)$	H	$H=\frac{hr_x}{b^2}$
$p(Pa)$	P	$P=\frac{p}{p_H}$
$t(s)$	$\overline{t}$	$\overline{t}=\frac{ut}{r_x}$
$W(s)$	W^*	$W^*=\frac{W}{E'r_x\ell}$
$u(m/s)$	U^*	$U^*=\frac{u\eta_o}{E'r_x}$
$\beta(N/m^2)$	$\overline{\beta}$	$\overline{\beta}=\frac{\beta r_x}{\eta_o u}$
$E'(N/m^2)$	G^*	$G^*=E'\alpha^*$

The residual term in Eq. (34) is obtained as:

$$F_i=\frac{1}{2\Delta X^2}\left\{\begin{array}{c}\left[\left(\frac{\overline{\rho}H^3}{\overline{\eta}}\right)_{i+1}+\left(\frac{\overline{\rho}H^3}{\overline{\eta}}\right)_i\right][g(\theta-1)]_{i+1}\\ -\left[\left(\frac{\overline{\rho}H^3}{\overline{\eta}}\right)_{i+1}+2\left(\frac{\overline{\rho}H^3}{\overline{\eta}}\right)_i+\left(\frac{\overline{\rho}H^3}{\overline{\eta}}\right)_{i-1}\right][g(\theta-1)]_i\\ +\left[\left(\frac{\overline{\rho}H^3}{\overline{\eta}}\right)_i+\left(\frac{\overline{\rho}H^3}{\overline{\eta}}\right)_{i-1}\right][g(\theta-1)]_{i-1}\end{array}\right\}$$
$$-\frac{\Upsilon}{\Delta X}\left\{(1-\Phi)\left[(\theta\overline{\rho}H)_{i+1}-(\theta\overline{\rho}H)_i\right]+(\Phi)\left[(\theta\overline{\rho}H)_i-(\theta\overline{\rho}H)_{i-1}\right]\right\}$$
$$-\Upsilon\frac{r_x(\theta\overline{\rho})_i}{b}S$$

where, $0.5\le\Phi\le1$, with the upper bound corresponding to forward differencing and the lower bound representing backward differences.

This expression is normally solved in EHL problems by means of the modified Newton–Raphson method [30]. F_i denotes the approximate solution of the equation, whereas $\overline{F}_i$ denotes the exact solution, obtained by applying Taylor's series.

$$\overline{F}_i=f(\overline{\theta}_{i-1},\overline{\theta}_i,\overline{\theta}_{i+1})=0$$
$$F_i=f(\theta_{i-1},\theta_i,\theta_{i+1})\neq0$$

and:

$$\overline{F}_i=F_i+\frac{\partial F_i}{\partial[g\theta]_{i+1}}\left\{[g\overline{\theta}]_{i+1}-[g\theta]_{i+1}\right\}+\frac{\partial F_i}{\partial[g\theta]_i}\left\{[g\overline{\theta}]_i-[g(\theta)]_i\right\}$$
$$+\frac{\partial F_i}{\partial[g\theta]_{i-1}}\left\{[g\overline{\theta}]_{i-1}-[g\theta]_{i-1}\right\}+e_t$$

$$\overline{F}_i=F_i+\frac{\partial F_i}{\partial[g\theta]_{i+1}}\left[g_{i+1}(\overline{\theta}_{i+1}-\theta_{i+1})\right]+\frac{\partial F_i}{\partial[g\theta]_i}\left[g_i(\overline{\theta}_i-\theta_i)\right]$$
$$+\frac{\partial F_i}{\partial[g\theta]_{i-1}}\left[g_{i-1}(\overline{\theta}_{i-1}-\theta_{i-1})\right]+e_t$$

If the truncation error (e_t) is assumed to be negligible and $\Delta\theta_n=g_n(\overline{\theta}_n-\theta_n)$, then:

$$-F_i=\frac{\partial F_i}{\partial[g\theta]_{i+1}}\Delta\theta_{i+1}+\frac{\partial F_i}{\partial[g\theta]_i}\Delta\theta_i+\frac{\partial F_i}{\partial[g\theta]_{i-1}}\Delta\theta_{i-1}$$

Now, the Jacobian terms (J) can be expressed as:

$$J_i=\frac{\partial F_i}{\partial[g\theta]_i}$$

Therefore:

$$-F_i=J_{i,i+1}\Delta\theta_{i+1}+J_{i,i}\Delta\theta_i+J_{i,i-1}\Delta\theta_{i-1}$$

A Gauss–Seidel iteration technique can be used to solve this, where the super-script k denotes the loop count within the fractional film's iterative process:

$$\Delta\theta_i^k=\frac{-F_i-J_{i,i-1}\Delta\theta_{i-1}^k-J_{i,i+1}\Delta\theta_{i+1}^k}{J_{i,i}}$$

$$\Delta\theta_i^k=\frac{-J[3]-J[0]\Delta\theta_{i-1}^k-J[2]\Delta\theta_{i+1}^k}{J[1]}$$

Appendix A4

See Tables 1–3.

Table 2
Material properties.

Surface roughness, Ra (μm)	0.4
Modulus of elasticity (Gpa)	209
Poisson's ratio (ν)	0.33

Table 3
Lubricant properties.

Lubricant type	75W-90BO
Dynamic viscosity at 20 °C (Pa s)	0.0115
Density at 20 °C (kg m^{-3})	1500
Pressure viscosity coefficient, α_o (GPa^{-1})	0.12
Temperature viscosity coefficient, β^* (°C^{-1})	0.04
Specific heat capacity, C_p (J kg^{-1} °C^{-1})	2.2
Thermal conductivity, k (W °C^{-1} m^{-1})	0.145

Table 1
Gear geometry and input shaft speed.

Parameter	First gear wheel	Second gear wheel	Third gear wheel	Fourth gear wheel	Fifth gear wheel	Sixth gear wheel	Reverse gear wheel
Inertia (kg m^2)	0.0040–0.0043	0.0020–0.0023+0.010–0.02 (second output shaft)	0.0010–0.0013	0.00060–0.00063	0.00045–0.00048	0.00035–0.00038	0.0030–0.0033
Base radius (mm)	55–60	50–55	40–45	35–40	30–35	30–35	55–60
Number of teeth (gear wheel)	40–43	40–43	35–38	25–27	30–33	26–28	34–37
Gear module (mm)	2.8–3.1	2.2–2.5	2.1–2.4	2.0–2.3	1.9–2.2	2.0–2.3	3.2–3.5
Face width (mm)	17–20	17–20	17–20	17–20	15–18	17–20	17–20
Helix angle (°)	25–27	31–33	31–33	31–33	31–33	31–33	19–21
Normal pressure angle (°)	19–21	18–20	18–20	16–18	16–18	16–18	18–20
Input shaft speed (rpm)	800 (nominal)+fluctuating component						

References

[1] Grubin AN. Contact stresses in toothed gears and worm gears. Book 30 CSRI for Technology and Mechanical Engineering, Moscow DSRI Trans. 1949:337.
[2] Dowson D, Higginson GR. A numerical solution to the elastohydrodynamic problem. Journal of Mechanical Engineering and Science 1959;1:6–15.
[3] Cameron A, Gohar R. Theoretical and experimental studies of the oil film in lubricated point contact. Proceedings of the Royal Society Series A 1966;291:520–36.
[4] Snidle RW, Evans HP. Elastohydrodynamics of gears. Tribology Series (Elsevier Science 1997;32:271–80.
[5] De la Cruz M, Theodossiades S, Rahnejat H. An investigation of manual transmission rattle. Proceedings of the Institution of Mechanical Engineers, Part K: Journal of Multi-body Dynamics 2010;224:167–81.
[6] Evans CR, Johnson KL. Regimes of traction in EHD lubrication. Proceedings of the Institution of Mechanical Engineers, Part C: Journal of Mechanical Engineering Science 1986;200:313–24.
[7] Gohar R, Rahnejat H. Fundamentals of tribology. London: Imperial College Press; 2008.
[8] Greenwood JA, Tripp J. The contact of two nominally flat rough surfaces. Proceedings of the Institution of Mechanical Engineers, Part C: Journal of Mechanical Engineering Science 1970-71;185:625–33.
[9] Li S, Kahraman A. A transient mixed elastohydrodynamic lubrication model for spur gear pairs. Transactions of ASME, Journal of Tribology 2010132 2010.
[10] Wang KL, Cheng HS. A numerical solution to the dynamic load, film thickness and surface temperatures in spur gears, Part I—Analysis. ASME Journal of Mechanical Design 1981;103:177–87.
[11] Wang KL, Cheng HS. A numerical solution to the dynamic load, film thickness and surface temperatures in spur gears, Part II—Results. ASME Journal of Mechanical Design 1981;103:188–94.
[12] Johnson KL, Greenwood JA. Thermal Analysis of an Eyring fluid in elastohydrodynamic traction. Wear 1980;61:353–74.
[13] Olver AV, Spikes HA. Prediction of traction in elastohydrodynamic lubrication. Proceedings of the Institution of Mechanical Engineers, Part J: Journal of Engineering Tribology 1998;212:321–32.
[14] Hua DY, Khonsari M. Application of transient elastohydrodynamic lubrication analysis for gear transmissions. STLE Tribology Transactions 1995;38: 905–13.
[15] Brancati R, Rocca E, Russo R. A gear rattle model accounting for oil squeeze between the meshing gear teeth. Proceedings of the Institution of Mechanical Engineers, Part D: Journal of Automobile Engineering 2005;219:1075–83.
[16] Tangasawi O, Theodossiades S, Rahnejat H. Lightly loaded lubricated impacts: idle gear rattle. Journal of Sound and Vibration 2007;308:418–30.
[17] De la Cruz, M, Theodossiades, S and Rahnejat, H Transmission Rattle: An Air and structure-borne Phenomenon. Proceedings of the Seventh European Nonlinear Oscillations Conference (ENOC-2011), 2011, Rome, Italy.
[18] Elrod HG. A cavitation algorithm. Trans. Asme Journal of Lubrication Technology 1981;103:50–354.
[19] Jakobsson B, Floberg L. The finite journal bearing considering vaporisation. Transactions of Chalmers University of Technology 1957.
[20] Olsson KO. Cavitation in dynamically loaded bearings. Trans. of Chalmers University of Technology; 1965.
[21] Houpert L. New results of traction force calculations in elastohydrodynamic contacts. Transactions of ASME, Journal of Tribology 1985;185:241–8.
[22] Karthikeyan B, Teodorescu M, Rahnejat H, Rothberg S. Thermo-elastohydrodynamics of grease lubricated concentrated point contacts. Proceedings of the Institution of Mechanical Engineers, Part C: Journal of Mechanical Engineering Science 2010;223:683–95.
[23] Stribeck, R. Die Wesentliechen Eigenschaften der Gleit und Rollenlager. Z. Ver. Dt. Ing. 1902;46;38:1341–1348,1432–1438 and 1902;46;39: p. 1463–70.
[24] Teodorescu M, Taraza D, Henein NA, Bryzik W. Simplified Elasto-Hydrodynamic Friction Model of the Cam Tappet Contact. SAE Transactions—Journal of Engines 2003;2003-01-0985:1271–82.
[25] Teodorescu, M, Balakrishnan, S and Rahnejat, H Integrated Tribological Analysis within a Multi- physics Approach to System Dynamics, Life Cycle Tribology—Proceedings of the 31st Leeds-Lyon Symposium on Tribology, Leeds, UK 7th–10th September 2004, Tribology and Interface Engineering Series. 2005;48: p. 725–37.
[26] Sasaki T, Mori H, Okino N. Fluid lubrication theory of roller bearings. Transactions on ASME, Journal of Basic Engineering 1962.
[27] Rahnejat H. Computational modelling of problems in contact dynamics. Engineering Analysis 1985;2:192–7.
[28] Rahnejat H. Multi-body Dynamics: Vehicles, Machines and Mechanisms. London, UK and Warrendale, PA, USA: Professional Engng. Publ. (IMechE) and SAE (Joint publishers); 1998.
[29] Gohar R. Elastohydrodynamics. London: Imperial College Press; 2001.
[30] Jalali-Vahid D, Rahnejat H, Jin ZM, Dowson D. Transient analysis of isothermal elastohydrodynamic point contacts. Proceedings of the Institution of Mechanical Engineers, Part C: Journal of Mechanical Engineering Science 2001;199:1159–73.
[31] Teodorescu M, Kushwaha M, Rahnejat H, Rothberg S. Multi-physics analysis of valve train systems: from system level to microscale interactions. Proceedings of the Institution of Mechanical Engineers, Part K: Journal of Multi-body Dynamics 2007;221:349–61.
[32] Chong WWF, Teodorescu M, Vaughan ND. Cavitation induced starvation for piston-ring/liner tribological conjunction. Tribology International. 2011;4(44): 483–97.
[33] Newmark NM. A method of computation for structural dynamics. Proceedings of the ASME, Journal of Engineering, Mechanical Division 1959;85(EM3): 67–94.
[34] Timoshenko S, Young DH, Weaver Jr WH. Vibration Problems in Engineering. New York: John Wiley & Sons; 1974.
[35] Vijayaraghavan D, Keith TG. Development and evaluation of a cavitation algorithm. Tribology Transactions 1989;32-2:225–33.
[36] Koronias G, Theodossiades S, Rahnejat H, Saunders T. Axle whine phenomenon in light trucks: a combined numerical and experimental investigation. Proceedings of the Institution of Mechanical Engineers, Part D: Journal of Automobile Engineering 2011;225:885–94.